International Journal of Legal Medicine (2019) 133:1549–1565
https://doi.org/10.1007/s00414-019-02040-1

ORIGINAL ARTICLE

Description of immature stages of *Thanatophilus sinuatus* (Coleoptera: Silphidae)

Pavel Jakubec[1] · Martin Novák[1] · Jarin Qubaiová[1] · Hana Šuláková[1,2] · Jan Růžička[1]

Received: 26 July 2018 / Accepted: 6 March 2019 / Published online: 16 March 2019

Abstract

Necrophagous beetles of genus *Thanatophilus* are well recognized as a group of beetles with a high potential utility in forensic entomology. They can be used to estimate postmortem interval (PMI) or validate the value for other groups of insects commonly encountered on human remains, like blowflies (Calliphoridae). However, reliable tools for instar and species identification of their larvae are needed as such information is crucial for allowing accurate PMI estimate. One of the most common species of the genus *Thanatophilus* in Europe is *Thanatophilus sinuatus*. This species occurs frequently on human remains and its larvae feed on decaying tissues throughout their development. Therefore, the larvae could become useful bioindicators for forensic entomology, although their current description does not allow reliable instar or species identification. Our goal was to provide morphological characters for species and instar identification of all larval stages of *T. sinuatus*. The larvae were obtained from laboratory rearing under controlled conditions (20 °C and 16:8 h of light/dark period). Qualitative and quantitative morphological instar and species-specific characters are described and illustrated. Additionally, we report observations of biological and developmental lengths for all stages of the species. We also compared these morphological characters with recent description of *T. rugosus* and provided an identification key of these two similar and often co-occurring species. We noticed that some characters for instar identification were shared between *T. sinuatus* and *T. rugosus* and were confirmed by comparison with larvae of *T. dentigerus* that they can be applied to other species of the genus.

Keywords *Thanatophilus sinuatus* · Larval instar identification · Morphology · Forensic entomology

Introduction

Necrophagous beetles are currently well established as a useful ecological group of insects in forensic entomology [1–3]. In some cases, they can provide us with estimates of the postmortem interval (PMI) as accurate as other groups of insects (e.g., blowflies (Calliphoridae)) [3], or at least they can allow for the validation of these estimates. The list of such species is long, but only fraction of them can be currently used as we lack the necessary basic information about their morphology (species and instar identification) and biology (thermal summation models).

Genus *Thanatophilus* Leach, 1815 belongs to the family Silphidae and contains 23 described valid species, distributed in Holarctic and Afrotropical Realms [4–6]. Most of these species occur in the North Hemisphere. Members of this genus share not only general appearance but also their very similar ecology. All known species are necrophagous in all active stages of development (larvae and adults), and they flourish on larger carrions of vertebrates, including humans. They appear to prefer earlier stages of decomposition and can commence to breed in the first 24 h after death [7]. These features make them a very promising group of beetles that could be used as bioindicators in the field of forensic entomology.

Adult specimens of this genus can be identified based on several available identification keys (e.g., [5, 6, 8–11]).

Electronic supplementary material The online version of this article (https://doi.org/10.1007/s00414-019-02040-1) contains supplementary material, which is available to authorized users.

✉ Pavel Jakubec
jakubecp@fzp.czu.cz

[1] Faculty of Environmental Sciences, Czech University of Life Sciences Prague, Kamýcká 129, 165 00 Praha – Suchdol, Czech Republic

[2] Police of the Czech Republic, Institute of Criminalistics Prague, P.O. Box 62/KUP, 170 89 Praha, Czech Republic

Table 1 Development length of *Thanatophilus sinuatus* at 20 °C and under 16:8 photoperiod

Stage	Egg	Instar I	Instar II	Instar III	Pupae
Mean length of development (in days)	2.83	2.97	3.26	19.30	13.56
Standard deviation (in days)	0.50	0.50	1.28	2.27	2.44
Number of observed specimens	46	41	38	24	20

Morphology of their larvae was mostly neglected in the past as was pointed out by Novák et al. [12] (Table 1). However, the recognition of their usefulness sparked a new interest, and the larvae of three member species (*T. capensis* Wiedemann, 1812 [junior synonym *T. mutilatus* Laporte de Castelnau, 1840], *T. micans* (Fabricius, 1794), and *T. rugosus* (Linnaeus, 1758)) were re-described in the past few years as a result [12, 13]. Along with morphological description of some of the larvae, the thermal summation models and instar identification models were developed [1, 7, 12–14]. The identification of eight species of this genus (*T. capensis*, *T. dispar* (Herbst, 1793), *T. lapponicus* (Herbst, 1793), *T. micans*, *T. rugosus*, *T. sagax* (Mannerheim, 1853), *T. sinuatus* (Fabricius, 1775), and *T. trituberculatus* (Kirby, 1837)) can also be currently verified by nucleotide sequences [1, 15–17]. All these information are essential to estimate time of colonization, which is widely used as a proxy for PMI.

Two out of the three recently described larvae belong to species occurring almost exclusively in Africa (*T. micans* was also reported from Yemen [4]), which is somewhat disproportional to the fact that the center of biodiversity of the genus *Thanatophilus* is in the Palearctic Region [4, 8]. To help cover this knowledge gap, we chose *Thanatophilus sinuatus* as our focal species. This beetle has a very wide trans-Palaearctic distribution (occurring across Europe, Asia, and North Africa) and is very common especially on the European continent [4, 18]. Adults and larvae of *T. sinuatus* were specifically recorded on 13.27% (26 out of 196) of human remains that were investigated by forensic entomologists in the Czech Republic (between the years 2003 and 2018) (Šuláková, unpublished data). Additionally, the species is known to replace blowflies, one of the crucial groups in forensic entomology, during the colder parts of the year [19]. These findings support our view that *T. sinuatus* is indeed an important species in the field of forensic entomology.

The need for its thorough re-description comes from the fact that it often co-occurs with *T. rugosus* [20, 21]. It is very difficult to separate these two species morphologically in the larval stages [22]. Only the third instar can be identified to the species level [12, 21]. Even though these species possess many similarities, it is generally not safe to assume the information they provide are interchangeable. This was already proven for *T. capensis* and *T. micans* and the potential error can be highly significant [1]. Finding unique morphological characters that would allow for precise identification is therefore important for potential practical applications.

Our re-description also aims to establish characters for larval instar identification. The main focus is on the qualitative characters that are independent of the larval size, as they provide more accurate insight. The advantage of these characters lies in the fact that they are much more straightforward to apply and only a microscope is necessary to detect them. This is in contrast to statistical methods where accurate measurements of several features are needed and data has to be processed in a specialized statistical software. We would like to test if such qualitative morphological characters are shared among other species of the same genus and compare them with characters that were already identified for larval instars of *T. rugosus* [12].

Material and methods

Rearing insects We collected adults of *T. sinuatus* by baited pitfall traps placed in an arable fields around Albeř (Czech Republic) (49°01′35.7″N 15°08′54.9″E) between the 16th and 20th of May, 2016. All collected beetle specimens were transported into the laboratory, identified to species, and sexed using identification key [9]. Adults of *T. sinuatus* were afterwards divided into groups of six, with equal number of male and female specimens. We followed a breeding protocol outlined in Novák et al. [12]. The breeding took place inside a climatic chamber with constant temperature and photoperiod regime (20 °C and 16 h of light followed by 8 h of dark) to mimic the natural environmental conditions during breeding season of this species.

The breeding boxes were inspected at least once a day, and new eggs were removed and placed in vertically positioned Petri dishes (9 cm diameter) filled up to 2/3 with soil and with a small piece of fish meat (*Scomber scombrus* Linnaeus, 1758) as described by Ridgeway et al. [1]. These Petri dishes were secured with rubber bands to prevent unwanted opening and were stored on trays for easier handling. Moisture was provided by submerging the bottom part of the dish into 3 cm layer of tap water for a few

seconds. The advantage of this breeding methodology lies in larger mass of soil regulating and stabilizing moisture. In addition to that, larvae are also provided with enough space to create their pupation chambers. The layer of soil, however, is very thin, thus forcing larvae to create pupal chambers right next to the wall, making them visible and easily observable without any disturbance.

Petri dishes with developmental stages were monitored every 24 h. Clutches of eggs from the same breeding pair and day were kept together, and hatching larvae were further separated based on the time they hatched or entered next developmental stage, allowing us to observe them and collect data about their development rate in different developmental periods (egg, 1st–3rd instar larvae and pupa). However, no more than three larvae were allowed to be held at the same time in the same dish to minimize the probability of cannibalism. To obtain representative specimens of each developmental stage, we removed few individuals that molted in previous 24 h and were fully sclerotized and we fixed them. The fixation process involved killing the specimen in ethyl acetate fumes, fixing it in hot water bath (90–95 °C), and storing in 75% alcohol solution.

Optical imaging The fixed specimens were cleared from soil and food particles by fine brush and placed in Digital Ultrasonic Cleaner PS-06A for a short period of time (up to 1 min, depending on the fragility of the specimen and its dirtiness). To improve the visibility of internal parts, we detached the heads of some specimens and boiled them in 10% potassium hydroxide (KOH). In case this process failed, to clear the specimen to a desirable level, we bleached it in 4% hydrogen peroxide to remove excess pigments and prevent the specimen from further loss of firmness by the effect of KOH. Images of external morphology were taken while specimens or their body parts were submerged in ethanol or glycerol to prevent drying. Glycerol additionally improves image quality by its favorable optical properties and by stabilizing the sample due to its viscosity. Images were taken by Canon macro photo lens MP-E 65 mm on a Canon 550D body, mounted on automated macro rail for focus stacking (Cognisys StackShot). Smaller details were photographed using Olympus BX53 microscope with Olympus DP73 digital camera. The sets of pictures were consequently stacked into a final image with a high depth of field in Zerene Stacker 1.04 by Zerene Systems LLC.

Electron imaging Fine details of external morphology and body structure were examined at the Faculty of Science of Charles University in Prague by JSM-6380LV (JEOL) scanning electron microscope (SEM) with a high resolution of 3.0 nm (30 kW). The methodology follows Novák [23]. Before imaging, the specimens were first dehydrated through a series of increasing alcohol concentrations. The samples were transferred sequentially to 60%, 70%, 80%, 90%, and 95% alcohol for ca. 0.5 h each. Dehydrated samples were then dried by critical point drying method. Dry samples were subsequently attached to an aluminum disk target and coated with gold in Bal-Tec Sputter Coater SCD 050, to ensure conductivity.

Final images from both optical and electron imaging were compiled using GIMP ver. 2.8.16 graphic program; graphs were compiled using R ver. 3.4.1 statistical computing program.

Terminology and measurements Interpretation and terminology of larval and pupal descriptions follow Lawrence and Ślipiński [24]. To obtain precise measurements of key morphological structures, we photographed them under Olympus SZX16 stereo microscope and measured them by graphics program EidosMicro. Each morphological feature was measured on eight specimens of the same age, except in URI (seven specimens of the first instar larvae measured), URII (seven specimens of the first and third instar larvae measured), and URS (seven specimens of the first and six of the third instar larvae measured). The following abbreviations are used in the text:

AI	Length of antennomere I
AII	Length of antennomere II
AIII	Length of antennomere III
A1L	Length of abdominal segment I
A1W	Width of abdominal segment I
HL	Head length (without labrum)
HW	Head width (at the widest point)
LPI	Length of labial palpomere I
LPII	Length of labial palpomere II
MPI	Length of maxillary palpomere I
MPII	Length of maxillary palpomere II
MPIII	Length of maxillary palpomere III
N1L	Pronotal length
N1W	Pronotal width (at the widest point)
N2L	Mesonotal length
N2W	Mesonotal width (at the widest point)
N3L	Metanotal length
N3W	Metanotal width (at the widest point)
URI	Length of urogomphal segment I
URII	Length of urogomphal segment II
URS	Length of urogomphal terminal seta

N1L/W	Ratio of pronotal length to pronotal width
N2L/W	Ratio of mesonotal length to mesonotal width
N3L/W	Ratio of metanotal length to metanotal width
HW/HL	Ratio of head width to head length
A1L/W	Ratio of abdominal segment I length to abdominal segment width

Results

Biology

Females of *T. sinuatus* were able to reproduce under long day photoperiod of 16:8 h (light:dark phases) and at a temperature of 20 °C. They laid small clusters of eggs (7.72 ± 2.16 eggs per cluster (N = 18 egg clusters)) in the substrate. They were probably unable to reach the desired depth under our laboratory setup, resulting in the clutches being deposited at the very bottom of the breeding box.

Development from egg to adult took on average 41.85 ± 3.08 days. The mean duration of each developmental stage is given in Table 1. The first instar larvae started searching for food right after emerging from the egg and stayed very close to the food source even throughout the second and partly the third instar. During the third instar, they stopped feeding and dug up a pupation chamber where they subsequently turned into pupa after a few days. The third instar seems to be a critical period in the development of this species as many specimens were unable to transition into pupae. We observed that disturbance of the chamber before pupation (by other larvae or by human investigators) often resulted in its abandonment. Such larvae often resumed feeding and postponed pupation beyond the normal period or even died before reaching it.

We observed cannibalistic behavior, very likely also among the sibling larvae that were not driven by starvation, as the food was provided ad libitum.

Morphometry

As expected, most measured body parts grow isometrically (see Online Resource 1) (Fig. 1). However, certain characters grow allometrically. These are certain segments of urogomphi and labial palpi (Fig. 2 and 3). The best example of allometric growth in *T. sinuatus* larvae is a change in the length of the first and second labial palpomeres. The first segment grows in an approximately linear way, though the second segment stays the same and even shrinks in the third instar (Figs. 1a, b and 4o–q). The discrepancy in growth rates of these two segments translates into a proportional difference that can be used as an instar identification character. There is a similar relationship between the first and second segments of urogomphi. The trend is clearly visible from graphs of length ratios between those segments throughout the subsequent instars as shown on Fig. 3 a and b.

Our analysis suggests that head width (Fig. 2) could also be used for instar identification. We did not observe any overlap in the values among the instars, although there are some limitations of this method (see [12]).

Description of immature stages of *Thanatophilus rugosus*

Family SILPHIDAE Latreille, 1806

Subfamily Silphinae Latreille, 1806

Genus *Thanatophilus* Leach, 1815

Species *Thanatophilus sinuatus* (Fabricius, 1775)

Description of immature stages of *Thanatophilus sinuatus*

Larvae. **Body** (Fig. 4a–i):

Instar III (Fig. 4a, d, and g). Mean value of total length: 14.84 ± 1.72 mm. Campodeiform larvae, more or less fusiform, widest at the metathorax and slightly narrowing towards both ends. Slender body only slightly dorso-ventrally flattened. Head and all terga strongly sclerotized, and covered by vestiture of scattered setae. All terga on lateral margin with few long setae that can be clearly visible from above or below. All thoracic and abdominal tergites I to VIII laterally explanate, dark brown to black, with translucent paratergites, completely creamy-white pigmented on their distal ends (Fig. 4j). Thoracic paratergites rounded, abdominal paratergites small and pointed posteriorly with longest seta protruding in the direction of its apex. Ventral side of thorax mostly white. Ventral area of abdominal segment I poorly sclerotized, white, with dark pigmentation only in the central area of the medial sternite and far lateral edges of laterosternites. Sclerites of abdominal segments II to VIII anteriorly with light-pigmented rim, with dark medial sternites and speckled dark laterosternites divided from the former by narrow lighter area (Fig. 4d; sls). Segment II with two distinguishable white lines dividing medial sternite and laterosternites. Venter of segment IX and X uniformly brown. Posterior segments ventrally overall darker than anterior. *Instar II* (Fig. 4b, e, and h). Mean value of total length: 9.56 ± 1.20 mm. Paratergites of thorax and abdomen with translucent spots of light pigmentation that are the most visible on protergum, but never with full creamy-white pigmentation on the distal ends of paratergites (Fig. 4k). Abdominal segment II ventrally sclerotized with distinguishable white lines dividing medial sternite and laterosternites. Sternites of abdominal segments III to VIII with narrow rim of light pigmentation anteriorly (Fig. 4e; flr), otherwise uniformly dark. *Instar I* (Fig. 4c, f, and i). Mean value of total length: 6.21 ± 0.93 mm. All thoracic and abdominal tergites uniformly dark brown to black (Fig. 4l). Abdominal segment II ventrally sclerotized with

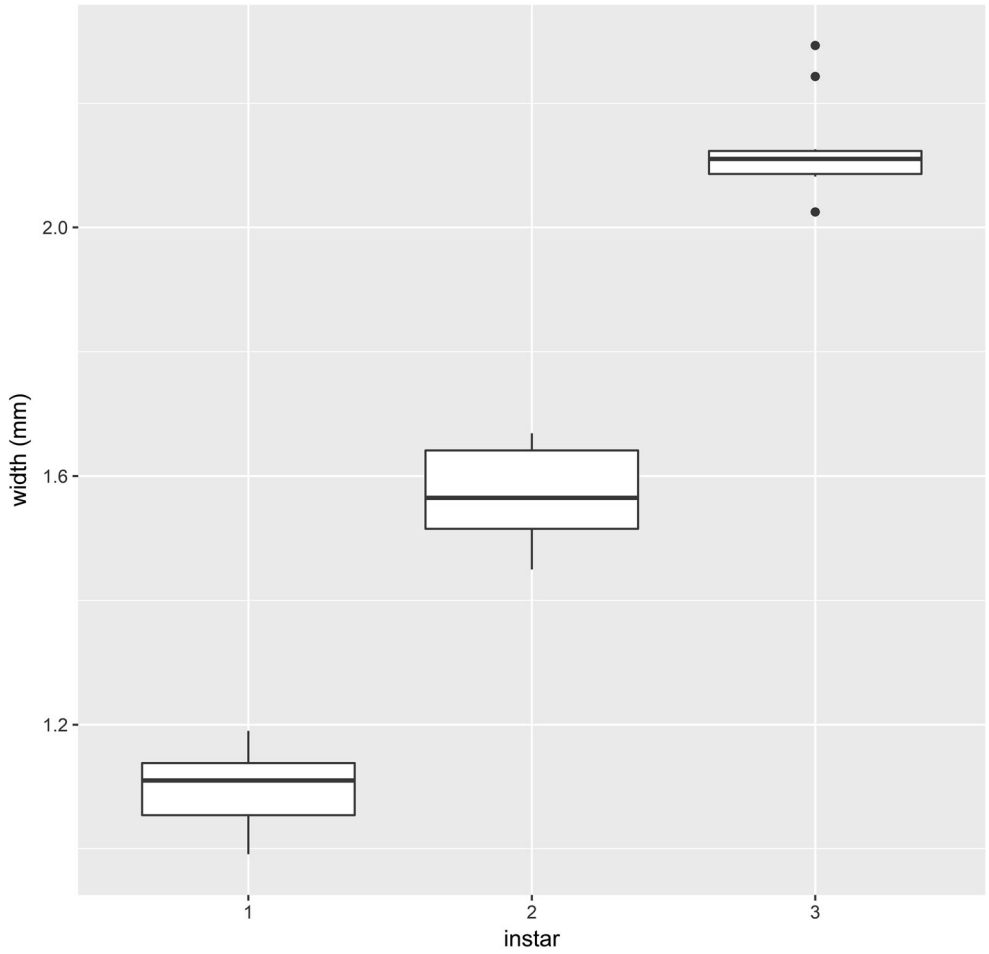

Fig. 1 Boxplots presenting the head width of all larval instars of *Thanatophilus sinuatus*. Horizontal lines within the boxes indicate median values; upper and lower boxes indicate the 75th and 25th percentiles, respectively; whiskers indicate the values with the 1.5 interquartile ranges; small, black dots are outliers

white lines dividing medial sternite and laterosternites. Sternites of abdominal segments III to VIII uniformly dark. Posterior segments ventrally overall darker and more sclerotized than anterior.

Head capsule (Fig. 5): *Instar III*. Prognathous and protracted; HW 2.13 ± 0.08 mm, HL 1.21 ± 0.16 mm, HW/HL 1.78 ± 0.24; reniform from ventral view; gena short, approximately half of the width of the head capsule in dorsal view. Head capsule dorsally covered with infrequent long setae mainly on labrum and clypeus and scattered short stout setae mainly on frons and vertex. Surface of frons and vertex covered by shallow cracks, with sparse convex nodules scattered along the cracklines mainly on vertex (Fig. 5c). Epicranial stem present, frontal arms V-shaped, with U-shaped base in 1/3 of their length from the stem (Fig. 5a; es, fa and f; esfa). Epicranial suture and epicranial stem of light coloration. Median endocarina absent. Six stemmata on each side of the head separated into two groups; four stemmata forming a trapezoid placed posteriorly behind antennal base and two stemmata placed ventrally under antennal base, parallel to the wider base of the trapezoid. Frontoclypeal suture absent; consisting only of linear anterior tentorial pits (Fig. 5a, f; atp), parallel to the posterior edge of clypeus. Clypeus subrectangular, ca. three and a half times as wide as long, partially covering mandibles in dorsal view; dorsally with six stout setae placed lengthwise anteriorly and many short thin setae, growing in elliptical pattern stretched over the area of clypeus. Labrum subtrapezoidal, dorsally with 8 long stout setae aimed anteriorly (two pairs on lateral-posterior margins and four on the anterior half of labrum). Labral apex double-arched, bearing two very short setae on the anterior edge (Fig. 6e; las). Epipharynx anteriorly covered with rows of bulbous processes and a pair of two large bulbous sensoria anteromedially (Figs. 5d and 6e; bs) and a pair of short conical spines placed laterally. Pharynx covered with rows of setae and spines which project up to posterior edge of clypeus, with oblique transverse cibarial plates (Fig. 5d; cp) in labral-clypeal membrane area and a pair of sensoria placed posteromedially behind these plates. Ventral mouthparts retracted, forming a maxillo-labial complex. Hypostomal rods absent. Ventral epicranial ridges present, roughly reaching beyond the level of the posterior edge of the maxillo-labial complex. Gular region short with gular sutures converging anteriorly. Tentorium consisting of a pair of sclerotized anterior arms (Fig. 5e–g; aa), laterally extended by fine hyaline lobes (Fig. 5e; ihl, ohl) in their basal 2/3, before the dorsal arms

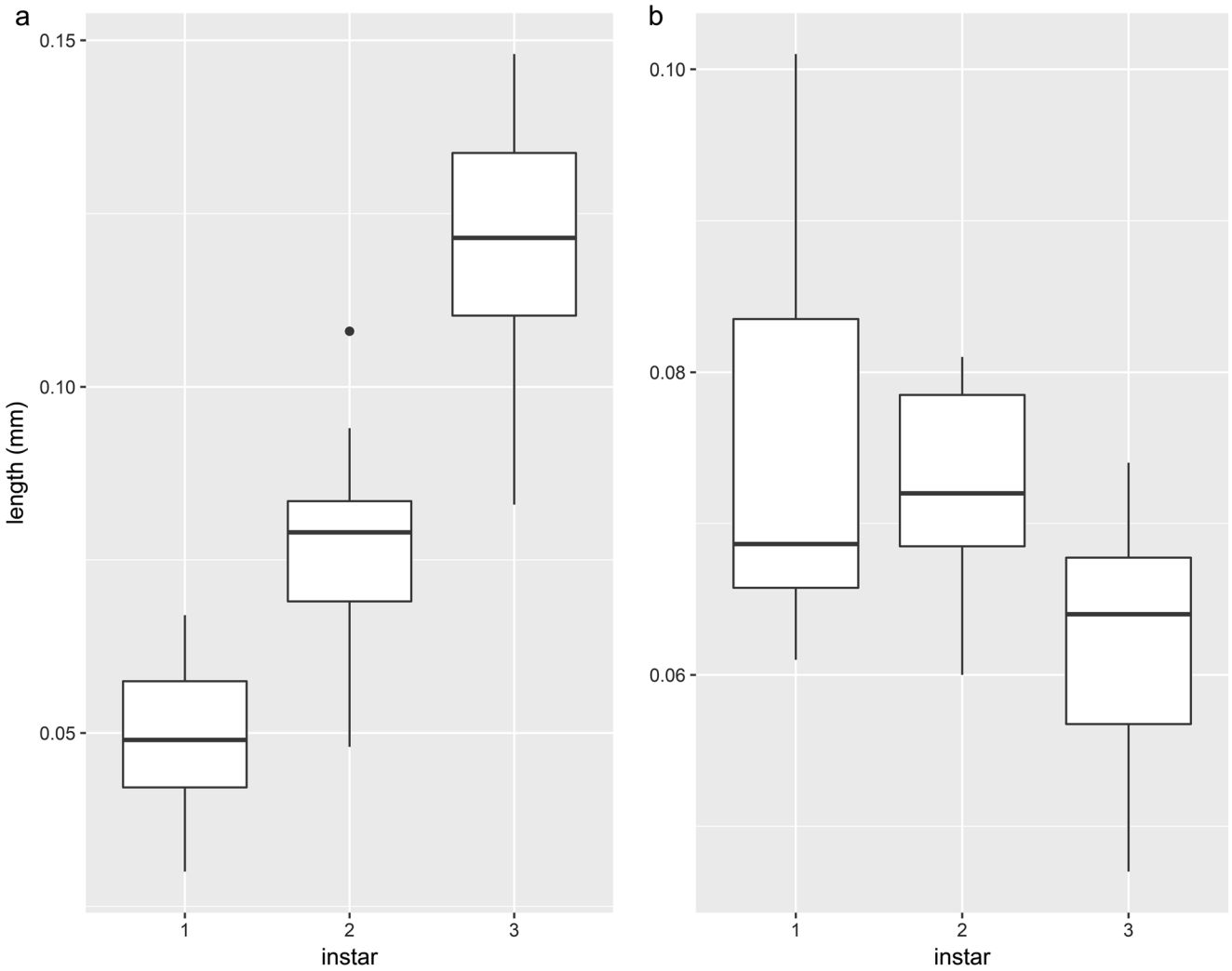

Fig. 2 Boxplots of labial palpomers length in all three larval instars of *Thanatophilus sinuatus*: palpomere I (**a**) and palpomere II (**b**). Horizontal lines within the boxes indicate median values; upper and lower boxes indicate the 75th and 25th percentiles, respectively; whiskers indicate the values with the 1.5 interquartile ranges; small, black dots are outliers

connecting to them; hyaline dorsal arms (Fig. 5e–g; da) connected to frons near the beginning of the U-shaped base of the frontal arms; and sclerotized posterior arms (Fig. 5e–g; pa) connected with posterior tentorial bridge (Fig. 5e; ptb). A pair of short sclerotized arms connected with filamentous secondary bridge (Fig. 5e–g; sb) growing dorsally from the middle of posterior arms. *Instar II*. HW 1.57 ± 0.08 mm; HL 1.02 ± 0.15 mm; HW/HL 1.57 ± 0.23. Vertex covered by scattered convex nodules (Fig. 5a). *Instar I*. HW 1.09 ± 0.06 mm; HL 0.70 ± 0.12 mm; HW/HL 1.62 ± 0.30. Vertex covered with dense small convex nodules (Fig. 5b).

Antennae (Fig. 7a–d): *Instar III*. Trimerous, inserted on lateral distal margin of gena; inserted in membranous socket. All antennomeres fully sclerotized and of more or less similar length (AI 0.33 ± 0.04 mm, AII 0.37 ± 0.03 mm, AIII 0.42 ± 0.04 mm). Antennomere I (Fig. 7a; amI) cylindrical, sloping laterally towards the longitudinal axis of the larva, bearing several stout setae on its distal half. Antennomere II (Fig. 7a; amII) club shaped, wider on distal end, sloping laterally towards the longitudinal axis of the larva, bearing several stout setae unequally and scarcely scattered across the surface. Sensorium of antennomere II (Fig. 7c, d) placed on inner lateral area of its distal end together with three small but bulky sensilla lacking a socket (Fig. 7c; bs), placed ventrally from the sensorium, the longest and the shortest sensilla growing from the same base, closer to the third antennomere compared to the medium-sized sensilla. Sensorium egg-shaped with conical top, widest at the base, encircled by a sclerotized ring, closely annealing to the second antennomere; a circle of small button-like sensilla placed around the apex of the sensorium (Fig. 7d; cs), with another circle of small sensillar pits (Fig. 7c; sp) closer to the base. Antennomere III (Fig. 7a; amIII) placed on outer lateral area of antennomere II, bearing several stout setae mainly on its distal two thirds and 4 setae on its apex; 2 articulated

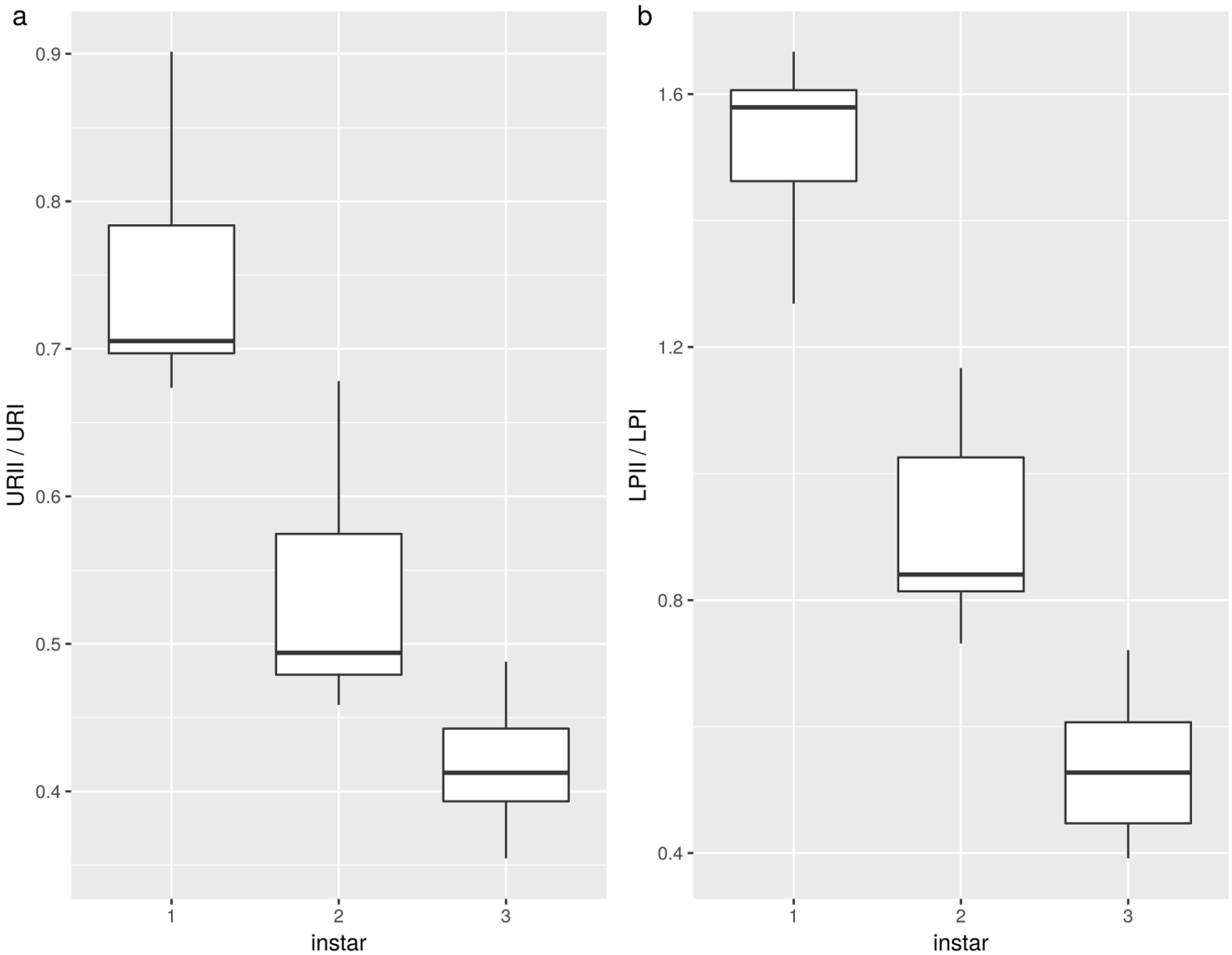

Fig. 3 Boxplots presenting the length ratio between urogomphi (URII and URI) (**a**) and labial segments (LPII and LPI) (**b**) of all three larval instars of *Thanatophilus sinuatus*. Horizontal lines within the boxes indicate median values; upper and lower boxes indicate the 75th and 25th percentiles, respectively; whiskers indicate the values with the 1.5 interquartile ranges; small, black dots are outliers

and short (Fig. 7b; sas), and 2 without articulation, one short and peg-like (Fig. 7b; sps), one long (Fig. 7b; las). *Instar II*. All antennomeres fully sclerotized, with first antennomere the shortest: AI 0.28 ± 0.04 mm, AII 0.37 ± 0.02 mm, AIII 0.40 ± 0.03 mm. *Instar I*. All antennomeres fully sclerotized, antennomere I shortest: AI 0.19 ± 0.02 mm; antennomere II and III of similar length: AII 0.27 ± 0.04 mm, AIII 0.34 ± 0.04 mm.

Maxilla (Figs. 4m and 6a). *Instar III.* Maxillary articulating areas present, completely unsclerotized. Lacinia and galea partly fused together. Cardo transverse, subtriangular, ca. two times wider than long, with one medium long seta ventro-laterally close to the base of stipes. Stipes sub-rectangular, longer than wide, ventrally bearing one long stout seta centrally, one long stout seta outer-laterally and several short setae roughly in between the two. Galea fixed; bearing two long setae outer-laterally and one short seta ventrally close to its base; with a brush of very dense setation on its apex (Figs. 4m and 6d; gb). Lacinia fixed, bearing eight to eleven visible stout spines on its outer lateral margin together with an apical lobe bearing a short cuticular projection composed of several shorter spines grown together (Fig. 4m; csp). Palpifer very short (Fig. 6a; mpf), sclerotized mainly on outer lateral margin. Maxillary palpus trimerous, palpomere I (Fig. 6a; mpI) cylindrical (MPI 0.11 ± 0.03 mm), ca. two times longer than wide; palpomere II (Fig. 6a; mpII) cylindrical (MPII 0.13 ± 0.02 mm), sloping laterally towards the longitudinal axis of the larva, palpomere III (Fig. 6a; mpIII) conically elongate (MPIII 0.22 ± 0.03 mm), longest of the palpomeres. Palpifer and palpomeres sparsely covered by several setae, palpomere III having a short stout seta in an articulated protuberance placed on outer-lateral edge of its base. The apex of palpomere III covered by numerous short blunt peg-like sensilla (Fig. 6b). *Instar II*. palpomere lengths: MPI 0.10 ± 0.02 mm; MPII 0.11 ± 0.02 mm; MPIII 0.23 ± 0.02 mm. *Instar I*. palpomere lengths: MPI 0.06 ± 0.01 mm; MPII 0.08 ± 0.01 mm; MPIII 0.19 ± 0.02 mm.

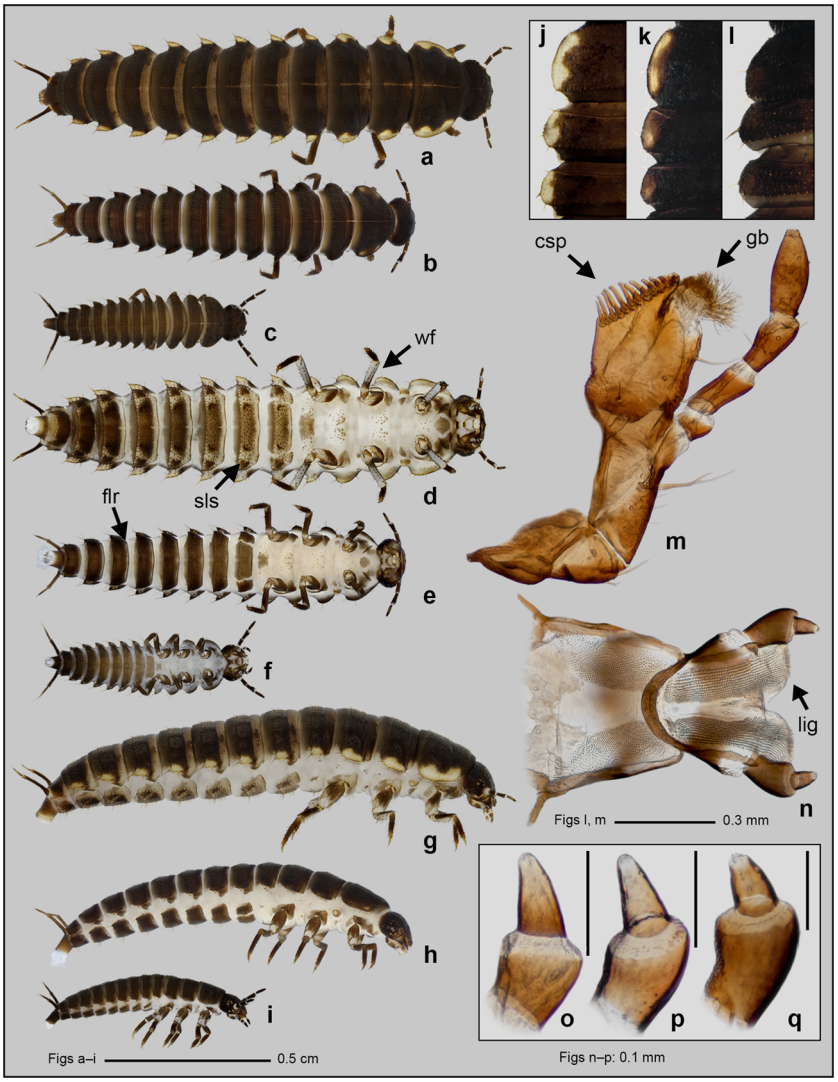

Fig. 4 *Thanatophilus sinuatus*: dorsal habitus of third instar (**a**); second instar (**b**) and first instar (**c**) larvae. Ventral habitus of third instar (**d**); second instar (**e**) and first instar (**f**) larvae. Lateral view of third instar (**g**); second instar (**h**) and first instar (**i**) larvae. Differences of pigmentation of paratergites among third instar (**j**); second instar (**k**) and first instar (**l**) larvae. Left maxilla of third instar larva in ventral view (**m**). Labium of third instar larva in dorsal view (**n**). Length differences among labial palpi of first instar (**o**); second instar (**p**) and third instar larvae (**q**). Abbreviations: csp – cuticular spines on lacinia; flr – light-pigmented rim on frontal edge of sternites of second instar larvae; gb – brush of setae on galea; lig – ligula; sls – speckled laterosternites of third instar larva; wf – white venter of femur of third instar larva

Labium (Figs. 4n–q and 6a, d) *Instar III*. Prementum, mentum and submentum are all sclerotized on their basal areas. Ligula bi-lobed (Figs. 4n and 6a, d; lig); each lobe along the sagittal plane covered dorsally by a group of numerous longitudinal lines of fine short setation and dense bulbous projections apically and centrally between the two groups; ventrally, a pair of long setae is present in the lateral parts of the central area of prementum (Fig. 6a; pm), as well as two pairs of shorter setae in between them centrally and a pair of shorter setae on the basal half. Labial palpus bimerous (Fig. 4q), LPI 0.12 ± 0.02 mm, LPII 0.06 ± 0.01 mm; basal palpomere (Fig. 6; lpI) club-shaped, sloping laterally towards the longitudinal axis of the larva, with no setation; distal palpomere (Fig. 6, lpII) conical, blunt, ca. 1/3 of the length of basal palpomere, sparsely covered in small thin peg-like sensilla on distal half and bearing a group of short blunt peg-like sensilla on its apex (Fig. 6c). Mentum (Fig. 6a; m) as long as wide, sub-oval, with dark pigmentation on its base; ventrally bearing two pairs of long setae on its posterior half. Submentum (Fig. 6a; sm) bearing a pair of long stout and several shorter thin setae, paired or irregularly scattered posterolaterally, alongside its sclerotized distal half when viewed ventrally. *Instar II*. Labial palpus bimerous (Fig. 4p), LPI 0.08 ± 0.02 mm, LPII 0.07 ± 0.01 mm. *Instar I*. Labial palpus bimerous (Fig. 4o), LPI 0.05 ± 0.01 mm, LPII 0.08 ± 0.01 mm.

Mandibles (Fig. 8) *Instar III*. Symmetrical (with slightly asymmetrical apex), simple without mola or prostheca, basal half consisting of wide triangular base in dorsoventral cross section, distal half more dorsoventrally flattened (Fig. 8a–d), apex consisting of two scissorial teeth lying obliquely, perpendicular to the plane of movement of the mandible; apical tooth (Fig. 8f; at) longer and serrated laterointernally, sub-apical tooth (Fig. 8f; sat) shorter, positioned dorsally towards the outer tooth and serrated lateroexternally towards the serrated area of the outer tooth. One long stout seta present laterodorsally on mandibular base (Fig. 8e; lds) and one short stout seta present outer-laterally in the mid-length of the

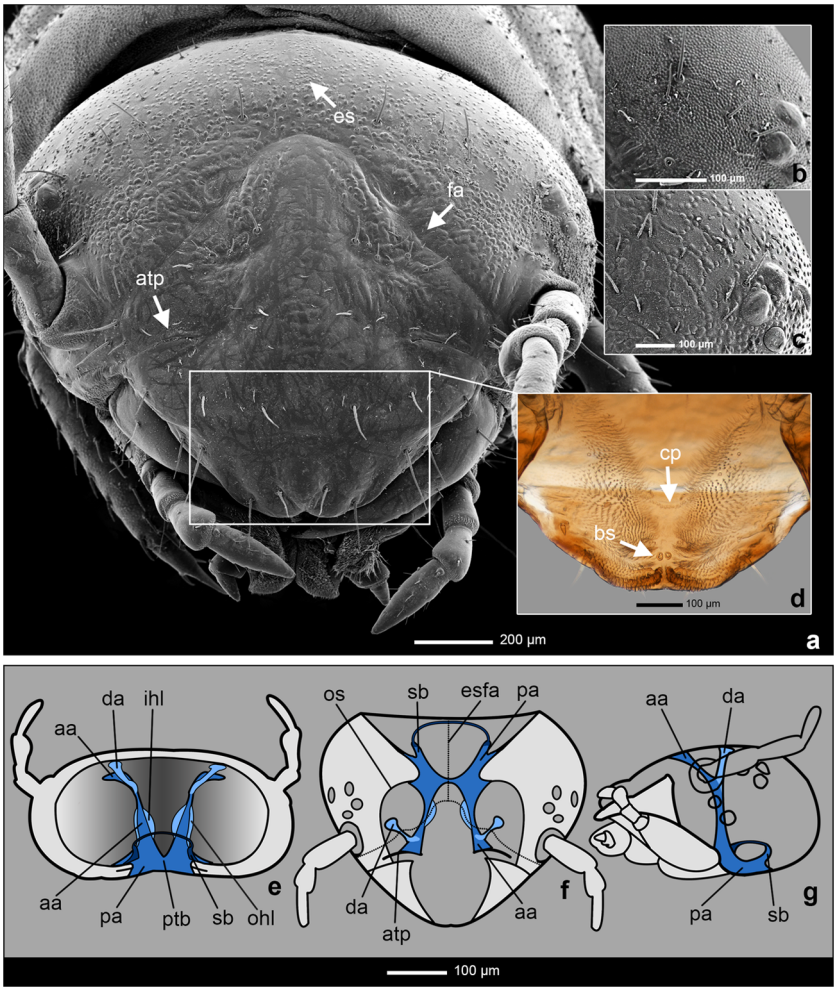

Fig. 5 *Thanatophilus sinuatus*: head of second instar larva in dorsal view (**a**); detail of head surface in dorsal view of first instar (**b**) and second instar (**c**) larva. Labrum, pharynx and epipharynx of third instar larva in ventral view (**d**). Tentorium of third instar larva in posterior (**e**); dorsal (**f**); and lateral (**g**) view (tentorium consisting of sclerotized features marked in dark blue and hyaline/membranous features marked in light blue). Abbreviations: aa – anterior arm; atp – anterior tentorial pit; bs – bulbous sensorium on epipharynx; cp – cibarial plates on pharynx; da – dorsal arm; esfa – epicranial stem with frontal arms (marked by dotted line); fa – frontal arm; ihl – inner hyaline lobe of anterior arms; ohl – outer hyaline lobe of anterior arms; os – occipital suture; pa – posterior arms; ptb – posterior tentorial bridge; sb – short sclerotized arms connected with filamentous secondary bridge growing dorsally from the middle of posterior arms

mandible (Fig. 8a, e; ms). Left mandible larger, covering the apex of the right mandible when clenched (Fig. 8e). In higher instars, the scissorial teeth of mandibles more worn out with apices and serrated areas more blunt (Fig. 8g). *Instar II.* and *Instar I.* same as Instar III.

Thorax (Fig. 4a–l) *Instar III.* Three-segmented, thoracic tergites divided by sagittal line; paratergites creamy white and translucent, slightly overlapping the body forming irregular semicircles (Fig. 4j). Protergum (N1W 3.41 ± 0.2 mm, N1L 1.43 ± 0.20 mm) suboval, wider posteriorly, rounded at posterolateral corners. Mesotergum (N2W 3.79 ± 0.23 mm; N2L 0.72 ± 0.08 mm) and metatergum (N3W 3.99 ± 0.24 mm; N3L 0.65 ± 0.06 mm) suboval, similar in shape and size. Venter of prothorax composed of short, semi-lens shaped, wider than long prosternum, subdivided into three dark-pigmented areas; lateral ones subtriangular, well sclerotized; medial area subrhomboid (or subpentagonal), semi-sclerotized. Ventrolateral areas of pro-, meso-, and metathorax composed of episternum and epimeron forming thin well-sclerotized strands and semi-sclerotized pre- and postcoxale. Lateral areas of thorax membranous, mesothorax bearing a large (relative to abdominal spiracles) annular spiracle with yellow colored peritreme (Fig. 4d, g) and bearing one long stout seta on its ventral posterior margin. The atrium (inner chamber) padded with shrub-like filtration hairs. Meso- and metasternum subdivided by transverse fold into membranous basisternum and sternellum. Basisternum covered by "freckles" of dark pigmentation, from which stout setae grow. Anterior ventral area of meso- and metathorax formed by membranous intersternite, laterally bounded with pair of sclerotized patches. *Instar II.* Thoracic paraterga with translucent spots of light pigmentation but never with full creamy-white pigmentation on the distal end; most visible on protergum (Fig. 4k). Protergum and mesotergum subdivided by sagittal line, metatergum subdivided by sagittal line on its anterior edge only. Protergum (N1W 2.31 ± 0.14 mm; N1L 0.95 ± 0.11 mm) suboval, wider posteriorly, rounded at posterolateral corners. Mesotergum (N2W 2.55 ± 0.15 mm; N2L 0.43 ± 0.06 mm) and metatergum (N3W 2.70 ± 0.13 mm; N3L 0.34 ± 0.07 mm) suboval, similar in shape and size. *Instar I.* Thoracic terga of uniform dark brown or black coloration (Fig. 4l). Protergum and mesotergum subdivided by sagittal line, metatergum subdivided by sagittal line on its anterior edge only. Protergum (N1W 1.46 ± 0.11 mm; N1L 0.57 ± 0.05 mm) semicircular, wider posteriorly, rounded at posterolateral corners. Mesotergum (N2W 1.56 ± 0.13 mm; N2L 0.28 ±

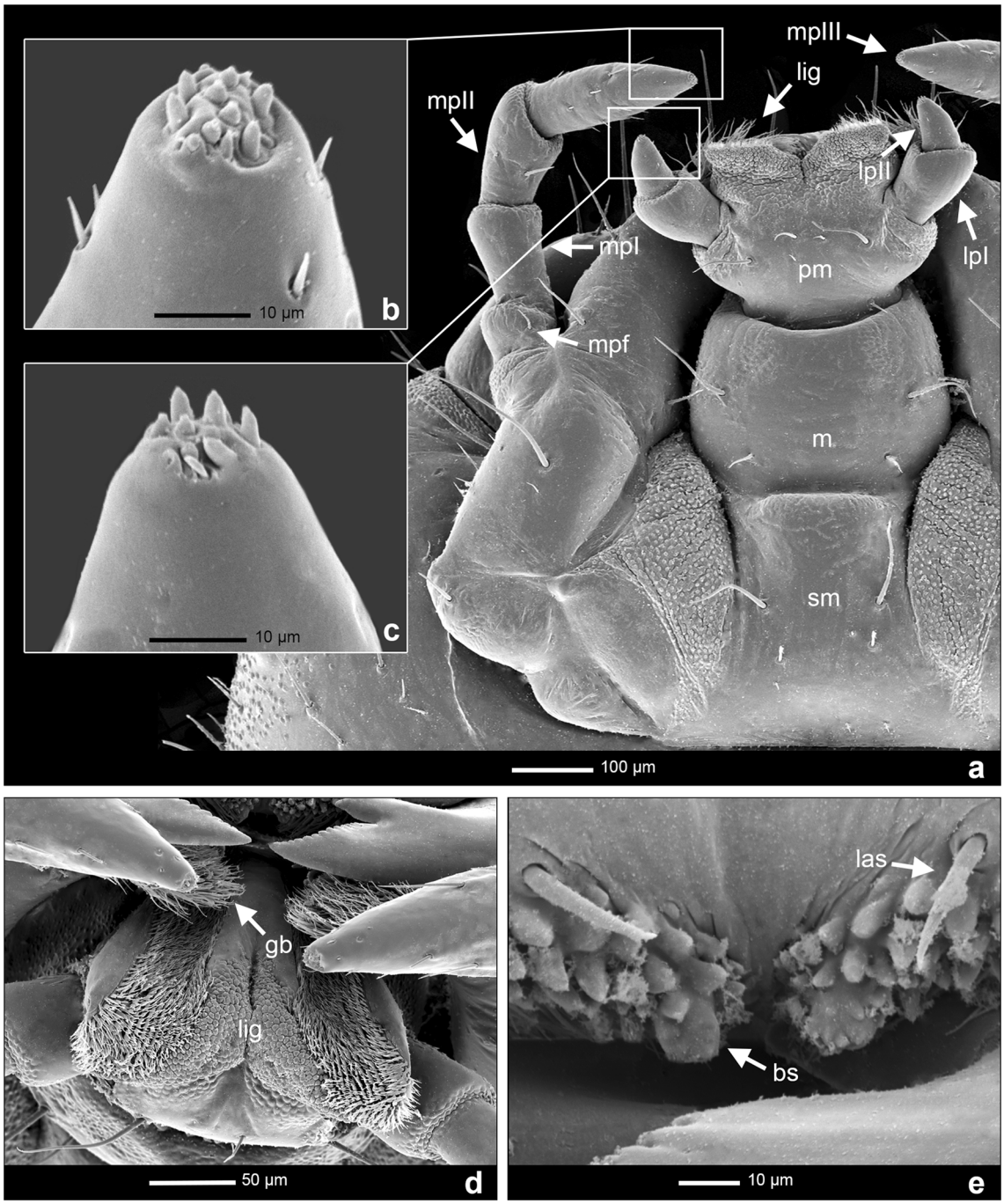

Fig. 6 *Thanatophilus sinuatus*: maxillo-labial complex of second instar larva in ventral view (**a**); apex of maxillary palpomere III (**b**) and labial palpomere II (**c**). Detail of ligula (**d**) and labral apex (**e**) in frontal view. Abbreviations: bs – bulbous sensorium on epipharynx; gb – brush of setae on galea; las – labral apical seta; lig – ligula; lpI – labial palpomere I; lpII labial palpomere II; m – mentum; mpI – maxillary palpomere I; mpII – maxillary palpomere II; mpIII – maxillary palpomere III; mpf – maxillary palpifer; pm – prementum; sm – submentum

0.04 mm) and metatergum suboval, similar in shape and size. Metatergum (N3W 1.65 ± 0.11 mm; N3L 0.23 ± 0.04 mm).

Abdomen (Fig. 4a–i) *Instar III.* Ten-segmented, tapering towards posterior end, segments I to VI dorsally subdivided by fine sagittal line anteriorly, on segment VI barely visible. Tergites of segments I to VIII subrectangular, narrow (A1W 3.93 ± 0.22 mm; A1L 0.50 ± 0.09 mm), similar in shape and coloration, with posteriorly pointed, creamy-white translucent paratergites. Tergite of segment IX subrectangular, bearing paired, well developed two-segmented urogomphi (Fig. 7g) that are inserted dorsolaterally. Basal segment of urogomphi narrow (URI 1.22 ± 0.21 mm), wider on proximal and distal

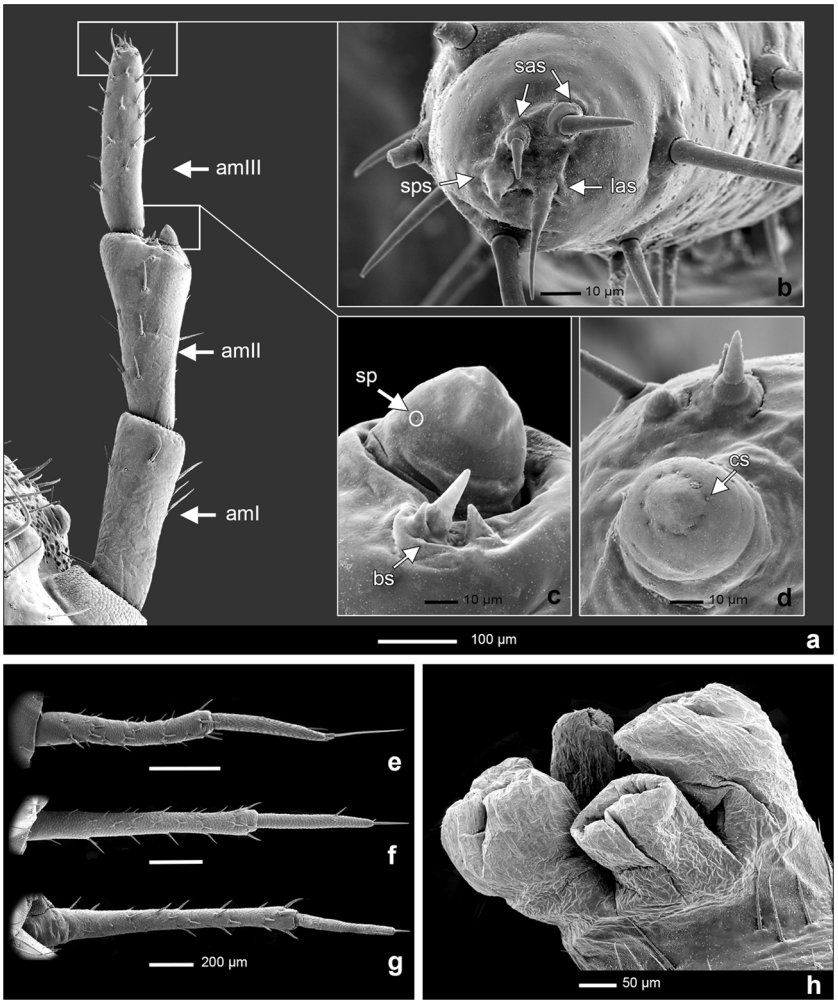

Fig. 7 *Thanatophilus sinuatus*: right antenna of third instar larva in ventral view (**a**); apex of second instar antennomere III (**b**); detail of third instar antennal sensorium and neighboring sensilla in lateral (**c**) and dorsal (**d**) view. Urogomphus of first instar (**e**), second instar (**f**), and third instar larva (**g**). Pygopod (**h**). Abbreviations: amI – antennomere I; amII – antennomere II; amIII – antennomere III; bs – bulky sensilla next to sensorium; cs – circle of button-like sensilla on sensorium; las – long apical sensilla; sas – short articulated sensilla; sp. – sensillar pit; sps – short, peg-like sensilla

ends, slightly bent posteromedially, bearing short stout setae. Distal segment slender (URII 0.52 ± 0.08 mm), ca. 2.3 time shorter than basal, cylindrical, with one short seta inserted on its apex (URS 0.12 ± 0.04 mm) and two prominent setae inserted on its body; the first thin and inserted dorsally slightly below the apex, the second stout and inserted innerventrolaterally on the apical third of the segment. Segment X dorsally subtrapezoidal forming a well sclerotized cylinder; distal central half of dorsal area with two longitudinal lines of white pigmentation; segment X holding the hold-fast organ (pygopod) with several eversible processes, sparsely covered in short spines on their distal ends (Fig. 7h). Segments I to VIII have membranous laterotergites with poorly sclerotized plates bearing annular spiracles with yellow colored peritreme, bearing no setae and placed on the venter of paratergites; the venter of segments I to VIII consists of subtrapezoidal, wider than long median sternite, margined by paired subtriangular laterosternites; median sternite and laterosternites of segment I membranous, but pigmented. Sternite of segment IX sub-rectangular. Spiracle on segment I largest of abdominal spiracles. *Instar II*. No abdominal tergites subdivided by sagittal line. Tergites of segments I to VIII sub-rectangular, narrow, A1W 2.67 ± 0.14 mm; A1L 0.26 ± 0.05 mm, similar in shape and coloration. Paratergites of abdomen with translucent spots of light pigmentation, but never with full creamy-white pigmentation on the distal ends. Venter of abdomen visually subdivided to median sternite and laterosternites on segments I and II only. Basal segment of urogomphi (Fig. 7f) narrow (URI 0.94 ± 0.11 mm), slightly bent posteromedially, distal segment slender (URII 0.50 ± 0.07 mm), cylindrical, ca. half as long as basal segment, with one seta inserted on the apex (URS 0.15 ± 0.01 mm) and bearing no seta on its base. *Instar I*. No abdominal tergites subdivided by sagittal line. Tergites of segments I to VIII sub-rectangular (A1W 1.63 ± 0.10 mm, A1L 0.16 ± 0.02 mm). Venter of abdomen visually subdivided to median sternite and laterosternites on segments I and II only. Basal segment of urogomphi (Fig. 7e) narrow (URI 0.55 ± 0.04 mm), bent posteromedially, distal segment slightly slender and cylindrical, but almost the same length as basal (URII 0.41 ± 0.07 mm), with long terminal seta (URS 0.24 ± 0.04 mm), and bearing no seta on its base.

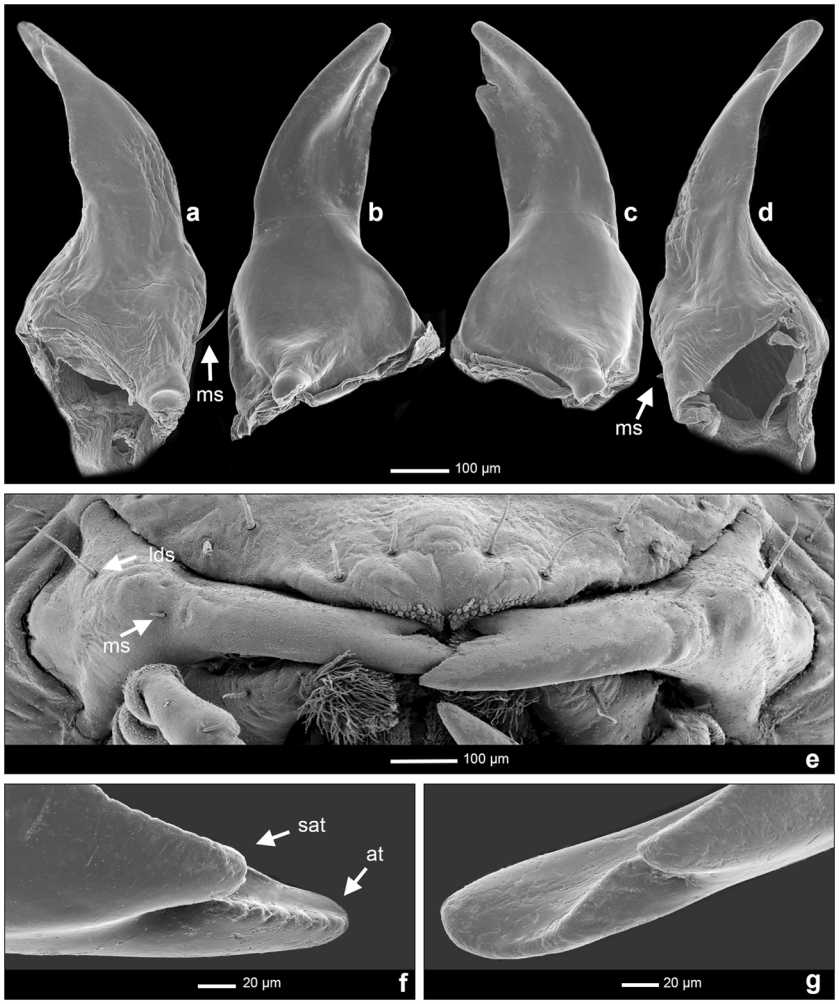

Fig. 8 *Thanatophilus sinuatus*: third instar larva right mandible in posterior (**a**) and ventral (**b**) view and left mandible in ventral (**c**) and posterior (**d**) view. Deposition of mandibles in head capsule of third instar larva in frontal view (**e**). Detail of scissoral teeth and their abrasion on right (**f**) and left (**g**) mandible of third instar larva in posterior view. Abbreviations: at – apical tooth; lds – seta on laterodorsal area of mandibular base; ms – seta on outer-lateral area in the mid-length of the mandible; sat – sub-apical tooth

Legs (Figs. 4a–i and 9) *Instar III*. Pentamerous including pretarsus, all pairs similar in shape and size. Coxa large, stout, covered by stout setae; with white pigmentation on the posterior and anterior area of the apex; coxal-trochanteal membrane reaching ca. 1/3 of longitudinal length. Trochanter small, subtriangular in lateral view, centrally white pigmented and sclerotized only basally and distally, covered by several stout setae of the same length as coxa and one seta ca. three to four times longer than the rest, placed ventrally on the distal end (Fig. 9a; ts). Femur cylindrical, dorsally sclerotized. Ventrally completely white (Fig. 4d; wf), bearing two longitudinal lines of sharp stout setae and a very long seta (ca. two times the length of neighboring setae) between these lines (Fig. 9a; fs); several other irregular longitudinal lines with shorter setation placed laterally and dorsally. Tibiotarsus ca. as long as femur, narrower, tapering towards distal end, bearing several longitudinal lines of stout sharp setae around its circumference followed by less regular lines of shorter setae. Pretarsus composed of a claw with stout base (Fig. 9b), ventrolaterally bearing a pair of stout setae placed in the mid-length of the claw. Common setae on coxa and trochanter generally thinner and slightly longer than stout strong setae on femur and tibiotarsus. *Instar II*. Femur cylindrical, fully sclerotized and dark pigmented. Claw (Fig. 9c) appears to be more slender than in instar III. *Instar I*. Claw (Fig. 9d) more slender than in instar III, with narrow base.

Pupa. (Fig. 10) Type of pupa: *adectica exarata libera*. Curved, ventrally concave. Length 22.2 mm. Coloration: cream white body with dark-brown setae.

Head capsule: Partially covered by protergum in dorsal view. Antennae short, extending laterally to half of the lateral length of protergum. Mouthparts visible in ventral view.

Thorax: Surface of protergum covered by numerous scattered short brown hairs, with a distinct line of hairs around its edge (Fig. 10; es) and with two pairs of long stout dark-brown setae on its anterolateral edge (Fig. 10; ps). Protergum oval, convex. Mesonotum less wide than metanotum, with distinct triangular protuberance posteromedially representing future scutellum (Fig. 10; sc). Wing pads (Fig. 10; wi) and rectangular elytra (Fig. 10; el) completely white and about the same length; wing pads reaching fourth abdominal segment. All pairs of legs free, visible in ventral view; femurs and tibiae

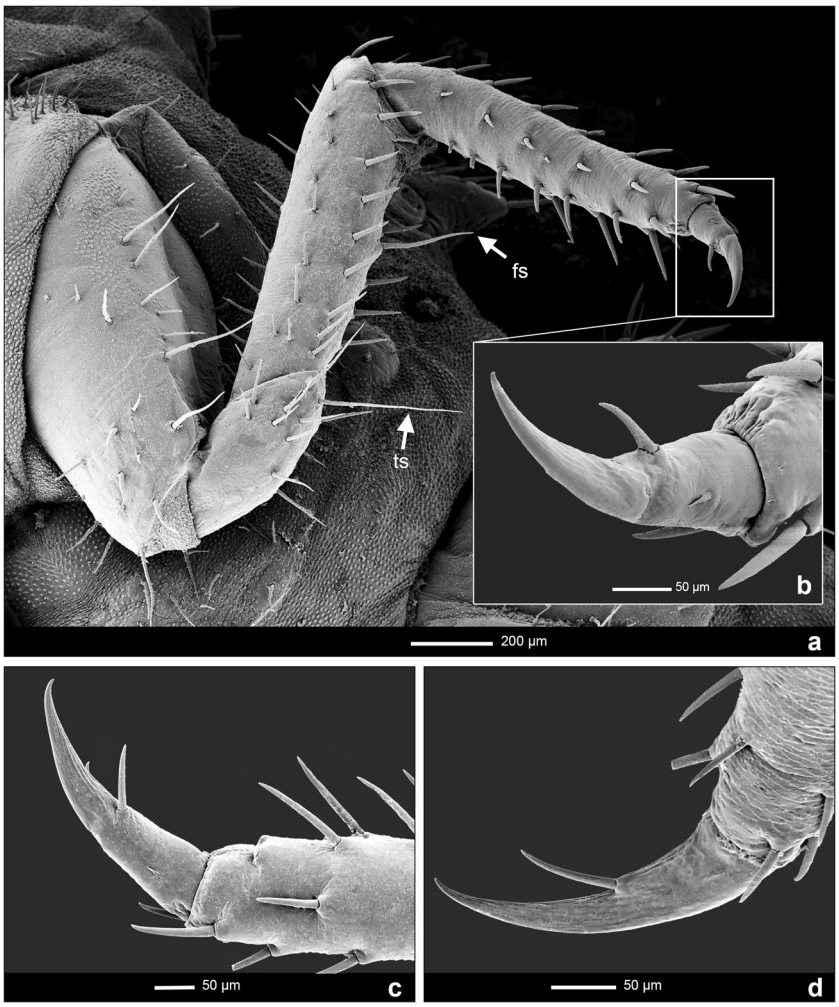

Fig. 9 *Thanatophilus sinuatus*: leg of third instar larva in lateral view (**a**). Detail of tarsal claw of third instar (**b**); second instar (**c**); and first instar (**d**) larva. Abbreviations: fs – longest seta of femur; ts – longest seta of trochanter

of metathoracic legs partially covered by wing pads, distal segments of tarsi extend to fifth abdominal segment when pupa straightened, if curved reaching seventh abdominal segment. Spiracles present on pleural areas of mesothorax.

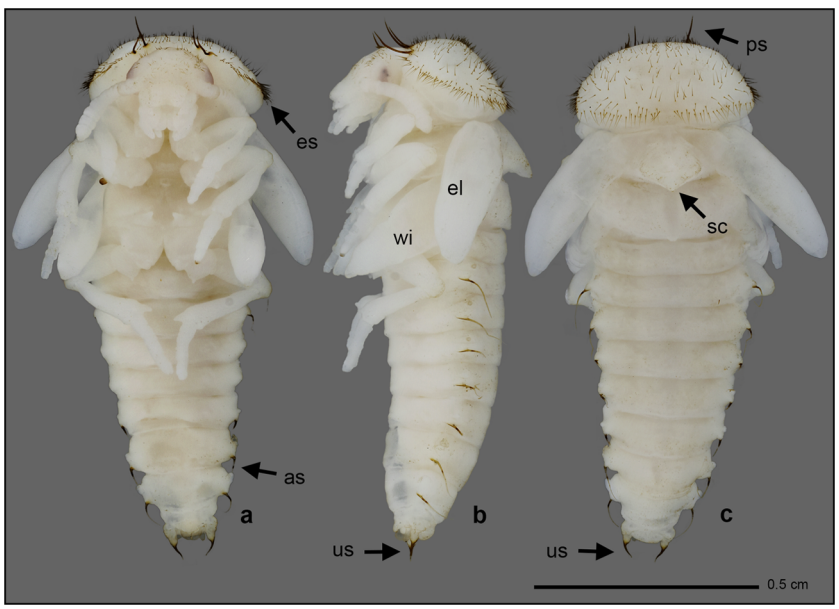

Fig. 10 *Thanatophilus sinuatus*: a day old pupa in ventral (**a**), lateral (**b**), and dorsal (**c**) view. Abbreviations: as – abdominal setae; el – future elytron; es – line of setae on the edge of protergum; ps – pronotal setae; sc – scutellum; us – urogomphal setae; wi – future wing

Abdomen: Abdominal segments sub-rectangular, wider than long. Segments II–VII bearing a pair of long stout brown setae (Fig. 10; as). Urogomphi on segment VIII short and bulky, white, with dark-brown apices bearing medium-long stout brown setae (Fig. 10; us). Spiracles present on abdominal pleural areas of segments I–VIII, on segments I-IV light-brown, otherwise white.

Identification key to larval instars of *T. sinuatus* and *T. rugosus*

1(2) Ventral part of femur on all legs white (Fig. 4d; wf); abdominal sclerites speckled with dark spots (Fig. 4d; sls). Anterior arms of tentorium with both, inner and outer hyaline lobes (Fig. 5e; aa, ohl, and ihl). = **Third instar**

2(1) Ventral part of femur on all legs dark and of similar shade as the rest of the femur (Fig. 4e, f); abdominal sclerites uniformly brown (Fig. 4e, f). Anterior arms of tentorium without or only with inner hyaline lobes (Fig. 5e; aa, ihl).

3(4) First segment of urogomphi ca. two times longer than the second (Fig. 7f); first segment of labial palpi longer and larger than the second segment (Fig. 4p). Anterior arms of tentorium with inner hyaline lobes only (Fig. 5e; aa and ihl). = **Second instar**

4(3) First segment of urogomphi less than 1.5 times longer than the second (Fig. 7e); first segment of labial palpi as long as the second and of similar bulk (Fig. 4o). Anterior arms of tentorium without any hyaline lobes (Fig. 5e; aa). = **First instar**

Identification key to *T. sinuatus* and *T. rugosus* larval instars

Third instar

1(2) Tergites dark brown, with paratergites fully creamy white on lateral ends (Fig. 4a, j). = ***T. sinuatus***

2(1) Tergites uniformly dark brown (Fig. 4a; [12]). = ***T. rugosus***

Second instar

1(2) Tergites dark brown, protergum (and possible other tergites) with lighter translucent spots on paratergites, never fully reaching lateral ends (Fig. 4b, k). = ***T. sinuatus***

2(1) All tergites uniformly dark brown (Fig. 4b; [12]). = ***T. rugosus***

First instar

1(2) Length of the first segment of labial palpus approximately 0.05 ± 0.01 mm, length of the first segment of maxillary palpus approximately 0.057 ± 0.01 mm. = ***T. sinuatus***

2(1) Length of the first segment of labial palpus approximately 0.08 ± 0.006 mm, length of the first segment of maxillary palpus approximately 0.105 ± 0.01 mm. = ***T. rugosus***

Discussion

Previous descriptions of developmental stages of *T. sinuatus* did not find any reliable characters that would allow for species identification of its larval instars [22, 25–27]. To our knowledge, the only reliable way of how to identify the larvae of *T. sinuatus* and *T. rugosus* was proposed in Novák at al. [12] and Frątczak-Łagiewska and Matuszewski [21]. However, both of them are limited to the third instar only, thus limiting its practical use. When dealing with larval material in forensic entomology, species identification is only the first part of the challenge as specimens have to be identified to instars as well. Without such knowledge, it is impossible to estimate the larval age accurately, which is crucial for the estimation of PMI in forensic entomology. Larval instars of *T. sinuatus* can be so far identified based on statistical models when three character measurements (distance between dorsal stemmata, and width of protergum and mesonotum) are provided [14]. This approach has its advantages and disadvantages as we argued previously [12]. Nonetheless, the morphological characters that we report in this article could be used to provide validation of the model or even replace it altogether.

Many of the characters for instar identification are shared between *T. sinuatus* and *T. rugosus.* The latter was already described in detail [12]. These characters are provided in the form of a dichotomous identification key in chapter **Identification key to *T. sinuatus* and *T. rugosus* larval instars** above. Additionally, *T. sinuatus* instars can be easily distinguished based on the coloration of their dorsal side. The third instar has white distal ends of almost all paraterga (Fig. 4j); the second instar has only small white marks in the middle of protergal paraterga (Fig. 4k). This pattern can sometimes be observed on other tergites of the second instar larvae, but it is individually variable. The first instar is always uniformly dark (Fig. 4l) and closely resembling the first instar of *T. rugosus*. However, they appear to differ in the length of the first segment of labial and maxillary palpi (Fig. 2).

We have gathered some evidence that qualitative characters for instar identification could be shared among the species of genus *Thanatophilus*. Besides the reported similarities between the species of *T. sinuatus* and *T. rugosus*, we also examined a limited larval material of *T. dentigerus*. All three species share the allometry in length of urogomphi segments (length of the first segment increases rapidly in the second instar, while the second segment does not). In addition, the femur of all legs becomes bicolored (dorsal side is darker than ventral part) in the third instar (the femurs of the first and second instars are monochromatic). On the other hand, the color of tergites remains consistent throughout the larval development, which is the same as in *T. rugosus*, but different from *T. sinuatus* as we discussed earlier. We could not confirm if the shape of tentorium changes between instars in *T. dentigerus* due to limited number of specimens in the first and second instar category.

Adults of *T. sinuatus* breed willingly when provided with food and material for egg laying. We did not encounter many setbacks following the breeding methodology suggested by

Ridgeway at al. [1]. The constant temperature and photoperiod (20 °C and 16/8 light cycle) in the climatic chambers, where the breeding took place, resulted in steady production of eggs; thus, we did not have to experiment with different environmental conditions. Nonetheless, this is in contrast to our experiences with its sibling species, *T. rugosus* [12], as it was unable to breed under the aforementioned conditions, and a change of light cycle to 12/12 was necessary to promote the production of eggs.

Both species (*T. sinuatus* and *T. rugosus*) were considered very similar in their occurrence patterns, both spatial and temporal, although, Frątczak-Łagiewska and Matuszewski [21] recently suggested that these two species differ in their seasonality in order to promote resource partitioning and therefore lower the resource competition between them. They observed the larvae of *T. sinuatus* occurring throughout the year up to August, but *T. rugosus* larvae were not recorded past mid-June. Our findings about different photoperiod requirements support their hypothesis stating that *T. sinuatus* is able to breed later in the season when the photoperiod is closer to 18:6 (light:dark) hours ratio, while *T. rugosus* restricts its breeding to earlier months of the year when the photoperiod is closer to 12:12 ratio.

The length of the development under the same temperature was very similar in both species, *T. sinuatus* (41.85 days) and *T. rugosus* (45.48 days) [12]. Both of them spend major parts of their life as third instar larvae and pupae but progress very rapidly through earlier stages (egg; first and second larval instars). The larvae of *T. sinuatus* hatch after approximately 3 days (2.83 days) at 20 °C. This period can be considered short compared to some larder beetles (genus *Dermestes*), which take around 8 days on average at the same temperature [28, 29]. However, the length of egg development at 20 °C is very similar to *T. mutilatus* [*T. capensis*] (3.58 days), *T. micans* (3.66 days), and *T. rugosus* (3.34 days) [1, 12]. This somewhat shared trait, among the members of the genus, could be caused by a number of factors including ecological ones. One of the possible explanations would be timing of the hatching of larvae in the optimal stage of carrion decay, as all these species share the preference for the same type of food source in the same stage of decomposition, even though they compete for it with other species (e.g., blowflies from family Calliphoridae) [1, 30–32].

We have observed several cases of cannibalism among the larvae of *T. sinuatus*. These cases were rather limited but they occurred in spite of the fact that food was provided ad libitum. Cannibalized specimens were often smaller or at some disadvantage (freshly molted specimens). It should also be noted that some of these specimens were probably related (siblings). We observed this pattern among the larvae of *T. rugosus* as well [12]. This behavior could be promoted by breeding conditions within the limited space of Petri dishes, but not necessarily so. Such behavior could also suggest some nutritional needs that are not met when feeding strictly on decaying meet. Thus, this could be compensated by cannibalism or predation of smaller competitors (like Calliphoridae) under natural conditions [31]. Further studies of feeding habits under natural conditions are nevertheless needed to provide support for either of such hypotheses.

It is a common belief among taxonomists that color is rarely a good character for identification, as it can change in time and vary among specimens. We have to partially agree with that statement as the color stability of *T. sinuatus* larvae can vary and is strongly affected by how the specimens were treated and preserved. During the preparation of larval specimens, we noticed that the larvae killed in ethyl acetate fumes and directly stored in alcohol tend to darken on otherwise white features such as distal ends of paraterga of third and second instars, ventral sides of femur in third instar, and all desclerotized parts on ventral side of all instars. The color change complicates not only instar identification but also species identification as darker specimens of *T. sinuatus* could be mistaken for *T. rugosus*.

The process of darkening is quite rapid and can be observed after only a few days of storage. To prevent this deterioration or at least prolong the color stability of the specimen, it is necessary to place them in hot water right after death and only then store them in alcohol. The water should be slightly below boiling point (90–95 °C) for desired effect to occur. Higher temperature could result in rupture of softer parts of cuticle and cause irreversible damage to the specimen. We also do not recommend skipping the first step of killing the animals in ethyl acetate fumes as they have tendency to curl and stiffen in that position when killed directly by hot water [33], which is inconvenient for handling and measuring of the specimens.

This article presents the re-description of all developmental stages of *T. sinuatus*, which is one of the most common and widely spread necrophagous species of beetles (see [4, 21, 30, 34, 35]). The utility of the species for the field of forensic entomology is undeniable as it has tight ecological association with its food source (development can take place only on carrion [36]) and is reported frequently from human remains or other large vertebrates (e.g., [2, 19, 37]). To increase the accessibility of the text to non-professional entomologists, we provide a key for instar identification of the *T. sinuatus* and its close relative *T. rugosus*. Additionally, we present the key for identification of those two species in every larval instar along with information about the biology of *T. sinuatus*, including the developmental length of all stages under constant laboratory conditions, and notes on its behavior. We believe that these results can help increase the value of this species as a bioindicator for forensic entomology.

Acknowledgments Thanks are due to Miroslav Hyliš (Praha, Czech Republic) for preparing our electron imaging samples and providing needed guidance at the SEM laboratory.

Funding The project was supported by the Ministry of the Interior of the Czech Republic (grant no. VI20152018027) and Internal Grant Agency of the Faculty of Environmental Sciences, CULS Prague (4211013123141).

Compliance with ethical standards

Conflict of interest H. Šuláková is an employee of Faculty of Environmental Sciences and Police of the Czech Republic.

Ethical approval All applicable international, national, and/or institutional guidelines for the care and use of animals were followed.

References

1. Ridgeway JA, Midgley JM, Collett IJ, Villet MH (2014) Advantages of using development models of the carrion beetles Thanatophilus micans (Fabricius) and T. mutilatus (Castelneau) (Coleoptera: Silphidae) for estimating minimum post mortem intervals, verified with case data. Int J Legal Med 128:207–220. https://doi.org/10.1007/s00414-013-0865-0
2. Charabidze D, Vincent B, Pasquerault T, Hedouin V (2016) The biology and ecology of Necrodes littoralis, a species of forensic interest in Europe. Int J Legal Med 130:273–280. https://doi.org/10.1007/s00414-015-1253-8
3. Midgley JM, Richards CS, Villet MH (2010) The utility of Coleoptera in forensic investigations. In: Amendt J, Goff ML, Campobasso CP, Grassberger M (eds) Current concepts in forensic entomology. Springer Netherlands, Dordrecht, pp 57–68
4. Růžička J (2015) Silphidae. In: Löbl I, Löbl D (eds) Catalogue of Palaearctic Coleoptera volume 2/1. Hydrophiloidea – Staphylinoidea, revised and updated edition. Brill, Leiden, pp 291–304
5. Anderson RS, Peck SB (1985) The insects and arachnids of Canada, part 13: the carrion beetles of Canada and Alaska (Coleoptera: Silphidae and Agyrtidae). Agriculture Canada, Ottawa
6. Navarette-Heredia JL (2009) Silphidae (Coleoptera) de México: diversidad y distribución. Universidad de Guadalajara, Guadalajara
7. Midgley JM, Villet MH (2009) Development of Thanatophilus micans (Fabricius 1794) (Coleoptera: Silphidae) at constant temperatures. Int J Legal Med 123:285–292. https://doi.org/10.1007/s00414-008-0280-0
8. Schawaller W (1981) Taxonomie und Faunistik der Gattung Thanatophilus (Coleoptera: Silphidae). Stuttg Beitr Naturkd A 351:1–21
9. Šustek Z (1981) Keys to identification of insects 2: carrion beetles of Czechoslovakia (Coleoptera: Silphidae). Zprávy Čsl Spol Ent Při ČSAV 2:1–47
10. Ratcliffe BC (1996) The carrion beetles (Coleoptera: Silphidae) of Nebraska. Bull Univ Nebr State Mus 13:1–100. https://doi.org/10.1093/aesa/90.3.399
11. Nikolaev GV, Kozminykh VO (2002) The carrion beetles (Coleoptera: Agyrtidae, Silphidae) of Kazakhstan, Russia and adjacent countries. Kazak Universiteti, Almaty
12. Novák M, Jakubec P, Qubaiová J, Šuláková H, Růžička J (2018) Revisited larval morphology of Thanatophilus rugosus (Coleoptera: Silphidae). Int J Legal Med 132:939–954. https://doi.org/10.1007/s00414-017-1764-6
13. Daniel CA, Midgley JM, Villet MH (2017) Determination of species and instars of the larvae of the afrotropical species of Thanatophilus Leach, 1817 (Coleoptera, Silphidae). Afr Invertebr 58:1–10. https://doi.org/10.3897/AfrInvertebr.58.12966
14. Frątczak K, Matuszewski S (2016) Classification of forensically-relevant larvae according to instar in a closely related species of carrion beetles (Coleoptera: Silphidae: Silphinae). Forensic Sci Med Pathol 12:193–197. https://doi.org/10.1007/s12024-016-9774-0
15. Woodcock TS, Boyle EE, Roughley RE, Kevan PG, Labbee RN, Smith ABT, Goulet H, Steinke D, Adamowicz SJ (2013) The diversity and biogeography of the Coleoptera of Churchill: insights from DNA barcoding. BMC Ecol 13:40. https://doi.org/10.1186/1472-6785-13-40
16. Pentinsaari M, Hebert PDN, Mutanen M (2014) Barcoding beetles: a regional survey of 1872 species reveals high identification success and unusually deep interspecific divergences. PLoS One 9: e108651. https://doi.org/10.1371/journal.pone.0108651
17. Sikes DS, Bowser M, Morton JM, Bickford C, Meierotto S, Hildebrandt K (2017) Building a DNA barcode library of Alaska's non-marine arthropods. Genome 60:248–259. https://doi.org/10.1139/gen-2015-0203
18. Jakubec P, Růžička J (2012) Distribution of open landscape carrion beetles (Coleoptera: Silphidae) in selected lowlands of the Czech Republic. Klapalekiana 48:169–189
19. Bonacci T, Greco S, Brandmayr TZ (2011) Insect fauna and degradation activity of Thanatophilus species on carrion in southern Italy (Coleoptera: Silphidae). Entomol Gen 33:63–70. https://doi.org/10.1127/entom.gen/33/2011/63
20. Jakubec P, Růžička J (2015) Is the type of soil an important factor determining the local abundance of carrion beetles (Coleoptera: Silphidae)? Eur J Entomol 112. https://doi.org/10.14411/eje.2015.071
21. Frątczak-Łagiewska K, Matuszewski S (2018) Resource partitioning between closely related carrion beetles: Thanatophilus sinuatus (F.) and Thanatophilus rugosus (L.) (Coleoptera: Silphidae). Entomol Gen 37:143–156. https://doi.org/10.1127/entomologia/2017/0352
22. von Lengerken H (1929) Studien über die Lebenserscheinungen der Silphini (Col.). XI-XIII. Thanatophilus sinuatus F., rugosus L. und dispar Hrbst. Z Morphol Ökol Tiere 14:654–666
23. Novák M (2017) Redescription of immature stages of central European fireflies, part 1: *Lampyris noctiluca* (Linnaeus, 1758) larva, pupa and notes on its biology (Coleoptera: Lampyridae: Lampyrinae). Zootaxa 4247:429–444
24. Lawrence JF, Ślipiński SA (2013) Australian beetles. Volume 1: morphology, classification and keys. CSIRO Publishing, Collingwood
25. von Lengerken H (1938) Beziehungen zwischen der Ernährungsweise und der Gestaltung der Mandibeln bei den Larven der Silphini (Coleopt.). Zool Anz 122:171–175
26. Paulian R (1941) Les premiers états des Staphylinoidea. Étude de morphologie comparée. Mémoires du Muséum Natl d'Histoire Nat. Nouv Ser 15:1–361
27. Xambeu PJV (1892) Moeurs et métamorphoses d'insectes (Suite). Annls Soc Linn Lyon 39:137–194
28. Coombs CW (1981) The development, fecundity and longevity of Dermestes ater Degeer (Coleoptera: Dermestidae). J Stored Prod Res 17:31–36. https://doi.org/10.1016/0022-474X(81)90029-1
29. Coombs CW (1979) The effect of temperature and humidity upon the development and fecundity of Dermestes haemorrhoidalis Küster and Dermestes peruvianus Laporte de Castelnau (Coleoptera: Dermestidae). J Stored Prod Res 15:43–52. https://doi.org/10.1016/0022-474X(79)90011-0

30. Dekeirsschieter J, Verheggen FJ, Haubruge E, Brostaux Y (2011) Carrion beetles visiting pig carcasses during early spring in urban, forest and agricultural biotopes of Western Europe. J Insect Sci 11:73
31. Matuszewski S, Bajerlein D, Konwerski S, Szpila K (2011) Insect succession and carrion decomposition in selected forests of Central Europe. Part 3: succession of carrion fauna. Forensic Sci Int 207: 150–163. https://doi.org/10.1016/j.forsciint.2010.09.022
32. Matuszewski S, Bajerlein D, Konwerski S, Szpila K (2010) Insect succession and carrion decomposition in selected forests of Central Europe. Part 2: composition and residency patterns of carrion fauna. Forensic Sci Int 195:42–51. https://doi.org/10.1016/j.forsciint.2009.11.007
33. Midgley JM, Villet MH (2009) Effect of the killing method on post-mortem change in length of larvae of Thanatophilus micans (Fabricius 1794) (Coleoptera: Silphidae) stored in 70% ethanol. Int J Legal Med 123:103–108. https://doi.org/10.1007/s00414-008-0260-4
34. Jakubec P, Růžička J (2017) Spatial distribution modeling of Thanatophilus sinuatus (Coleoptera: Silphidae) in the Czech Republic. In: 17th International Multidisciplinary Scientific GeoConference SGEM 2017. International Multidisciplinary Scientific Geoconference, Sofia, pp 875–882
35. Matuszewski S, Szafałowicz M (2013) Temperature-dependent appearance of forensically useful beetles on carcasses. Forensic Sci Int 229:92–99. https://doi.org/10.1016/j.forsciint.2013.03.034
36. Sikes D (2008) Carrion beetles (Coleoptera: Silphidae). In: Capinera JL (ed) Encyclopedia of entomology. Volume 1: A - C, 2nd edn. Springer, Berlin, pp 749–758
37. Matuszewski S, Frątczak K, Konwerski S, Bajerlein D, Szpila K, Jarmusz M, Szafałowicz M, Grzywacz A, Mądra A (2016) Effect of body mass and clothing on carrion entomofauna. Int J Legal Med 130:221–232. https://doi.org/10.1007/s00414-015-1145-y